Rapsyn mediates subsynaptic anchoring of PKA type I and stabilisation of acetylcholine receptor in vivo

Kyeong-Rok Choi[1], Marco Berrera[2], Markus Reischl[3], Siegfried Strack[1], Marina Albrizio[1], Ira V. Röder[1], Anika Wagner[1], Yvonne Petersen[1], Mathias Hafner[4], Manuela Zaccolo[2] and Rüdiger Rudolf[1,*]

[1]Institut für Toxikologie und Genetik, and [3]Institut für Angewandte Informatik, Karlsruhe Institute of Technology, Hermann-von-Helmholtz-Platz 1, 76344, Eggenstein-Leopoldshafen, Germany
[2]Institute of Neuroscience and Psychology, University of Glasgow, Glasgow G12 8QQ, UK
[4]Institut für Molekular- und Zellbiologie, Hochschule Mannheim, Paul-Wittsack-Strasse 10, 68163, Mannheim, Germany
*Author for correspondence (ruediger.rudolf@kit.edu)

Accepted 22 September 2011
Journal of Cell Science 125, 714–723

doi: 10.1242/jcs.092361

Summary

The stabilisation of acetylcholine receptors (AChRs) at the neuromuscular junction depends on muscle activity and the cooperative action of myosin Va and protein kinase A (PKA) type I. To execute its function, PKA has to be present in a subsynaptic microdomain where it is enriched by anchoring proteins. Here, we show that the AChR-associated protein, rapsyn, interacts with PKA type I in C2C12 and T-REx293 cells as well as in live mouse muscle beneath the neuromuscular junction. Molecular modelling, immunoprecipitation and bimolecular fluorescence complementation approaches identify an α-helical stretch of rapsyn to be crucial for binding to the dimerisation and docking domain of PKA type I. When expressed in live mouse muscle, a peptide encompassing the rapsyn α-helical sequence efficiently delocalises PKA type I from the neuromuscular junction. The same peptide, as well as a rapsyn construct lacking the α-helical domain, induces severe alteration of acetylcholine receptor turnover as well as fragmentation of synapses. This shows that rapsyn anchors PKA type I in close proximity to the postsynaptic membrane and suggests that this function is essential for synapse maintenance.

Key words: Neurotransmitter receptor recycling, A-kinase anchoring protein, Rapsyn, Skeletal muscle

Introduction

Metabolic stabilisation of acetylcholine receptors (AChRs) at the neuromuscular junction (NMJ) is dependent on muscle activity (Lomo and Rosenthal, 1972; Stanley and Drachman, 1981) as well as on postsynaptic signalling (Fambrough, 1979; Nelson et al., 2003; Shyng et al., 1991; Witzemann et al., 1987; Xu and Salpeter, 1997; Xu and Salpeter, 1999) and protein transport processes (Yampolsky et al., 2010b). Particularly, receptor recycling plays an important role in the activity-dependent regulation of AChR turnover (Akaaboune et al., 1999; Bruneau et al., 2005; Röder et al., 2008). To mediate efficient AChR recycling, the subsynaptic enrichment of a complex of AChR, myosin Va, and protein kinase A (PKA) type I was found to be essential (Röder et al., 2010; Rudolf et al., 2011; Yampolsky et al., 2010a). This fits with a long-proposed function of PKA type I in AChR stabilisation (Nelson et al., 2003; Shyng et al., 1991; Xu and Salpeter, 1997), which is probably mediated by neurogenic factors, such as α-calcitonin gene-related peptide (Nelson et al., 2003).

A missing link in this scenario has been the factor that mediates accumulation of PKA type I in proximity to the NMJ. Typically, PKAs are targeted to specific subcellular sites by means of A-kinase anchoring proteins (AKAPs) (Colledge and Scott, 1999). These are structurally heterogeneous proteins, which exhibit subcellular targeting sequences and PKA binding sites. In addition, most AKAPs also act as scaffold proteins by binding further factors, such as receptors, phosphatases etc. By that means, AKAPs act as signalling integrators that link PKA, effector molecules and signal modifiers in close proximity to the expected site of signal arrival (Colledge and Scott, 1999). Together with other mechanisms, this allows the cell to efficiently compartmentalise different cAMP-dependent processes and to maintain high signal specificity (Zaccolo, 2009). In most cases, AKAPs mediate binding to PKA regulatory subunits (PKA-R) through amphipathic α-helical sequences, which interact with an N-terminal stretch on PKA-R called the dimerisation and docking domain (DD domain) (Colledge and Scott, 1999). DD domains are specific for the different PKA-Rs known in mammals.

The receptor-associated protein of the synapse (rapsyn, also known as RAPSN) is a 43 kDa protein, which is strongly associated with AChRs at the NMJ and plays an important role in clustering of AChRs at the synapse (Frail et al., 1988; Gautam et al., 1995). From N- to C-terminus, it consists of a myristoylation site, seven tetratricopeptide repeats, an amphipatic α-helical stretch, a RING H2 domain and consensus sequences for PKC and PKA phosphorylation (Ramarao et al., 2001; Ramarao and Cohen, 1998). So far, the α-helical stretch (residues 299–331) has been described as important for AChR clustering (Ramarao et al., 2001; Ramarao and Cohen, 1998). In the light of our recent finding that a complex forms between recycling AChRs, myosin Va and PKA type I, we have investigated whether rapsyn is responsible for PKA localisation at the NMJ.

Journal of Cell Science

Results

In silico modelling predicts interaction between rapsyn amphipathic helix and PKA-RIα DD domains

Previously, rapsyn residues 298–331 were described as forming a coiled-coil domain including an amphipathic helix (Ramarao et al., 2001). Amphipathic helices are known to mediate interaction of AKAPs with PKA (for a review, see Colledge and Scott, 1999). In particular, the specificity determinants of AKAP10 binding to PKA-RIα (also known as PKRAR1A) were recently elucidated by the X-ray structure of the complex between the amphipathic helix and DD domains (Sarma et al., 2010). AKAP10 helix bound diagonally to the PKA-RIα DD domain homodimer. Four hydrophobic interaction pockets were characterised and they involved AKAP10 residues from the hydrophobic face of the amphipathic helix equally spaced on the sequence. Previously, the profile Hidden-Markov model (HMM) of the AKAP amphipathic helix motif that binds to PKA has been successfully employed to predict novel PKA anchoring proteins despite their low sequence identity (McLaughlin et al., 2011). We have used this approach to locate the PKA binding motif of rapsyn by alignment of its sequence to the profile HMM that is calculated from the alignment of 22 different PKA-binding AKAP sequences (McLaughlin et al., 2011) (Fig. 1A).

Under the assumption that rapsyn interacts with PKA in an AKAP-like manner, to characterise the interactions stabilising the complex we then modelled the complex between the rapsyn coiled-coil fragment and PKA-RIα on the basis of the X-ray structure of AKAP10 amphipathic helix bound to DD domains of PKA-RIα (Sarma et al., 2010) and of the corresponding sequence alignment (Fig. 1A). Due to missing template structures for residues 298–304, we modelled only rapsyn residues 305–331 as α-helix. Then, the complex was immersed in a water solvent box and 100 nanoseconds of molecular dynamics (MD) simulation under standard conditions were performed to test the stability of the complex and of the protein–protein interactions. Root square mean deviation (RMSD) fluctuated at about 0.2 nm and no conformational change or repositioning of the helix were observed within the investigated time frame. Interactions between PKA-RIα and rapsyn were mainly hydrophobic contacts between residues at the dimerisation interface of DD domains and residues from the hydrophobic face of the amphipatic helix, similar to those characterised in detail for AKAP10 (Sarma et al., 2010). Salt bridge interactions were observed between the lysine 311 of rapsyn (rapsyn-K311) and PKA-RIα-E17 as well as between rapsyn-K327 and PKA-RIα-E17′′ (on the opposite DD domain helix). Hydrophobic interactions were estimated for each residue on the basis of a contact surface calculation and averaged throughout the MD trajectory. Rapsyn residues with large contact surface (>0.40 nm^2) were A308, K311, A312, L315, A316, V319, L323 and K327 (Fig. 1B). PKA-RIα residues forming a large surface of contact with rapsyn were L13, E17, Q26, K30, I33 and

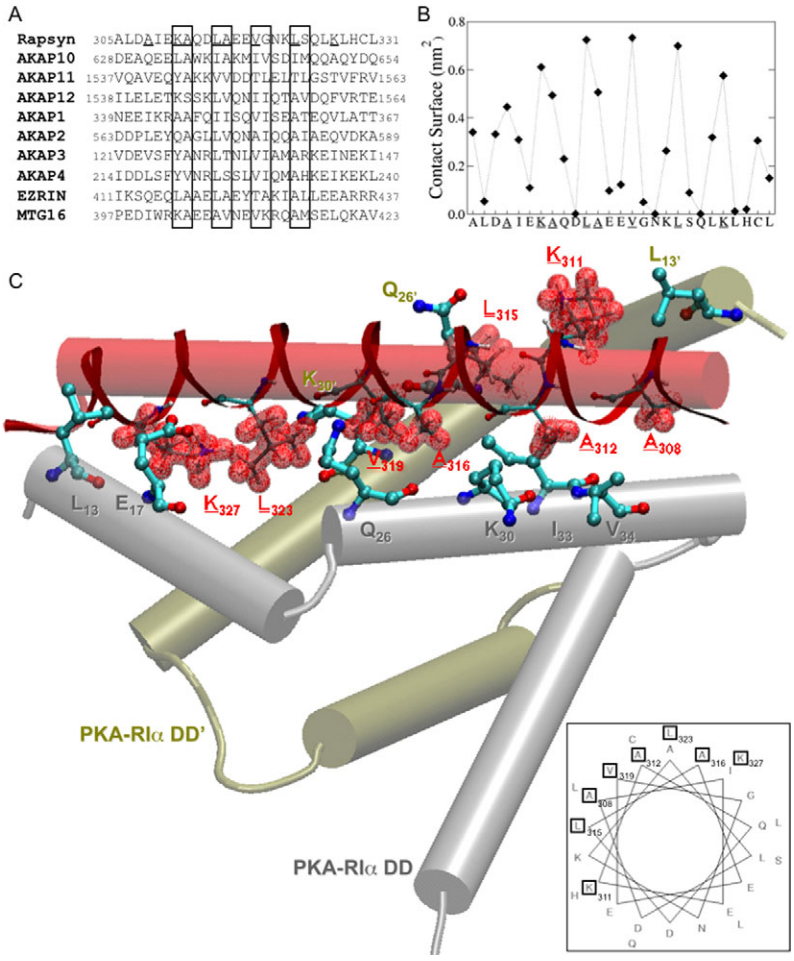

Fig. 1. In silico structural model of the complex between rapsyn α-helical domain and DD domain homodimer of PKA-RIα. (**A**) The sequence of rapsyn amphipathic helix (residues 305–331) was aligned with the AKAP10 amphipathic helix (residues 628–654) via profile HMM calculated from the sequence alignment from McLaughlin (McLaughlin et al., 2011). The sequence alignment of rapsyn with several dual-specificity AKAPs is shown. The residues lining the four interaction pockets as defined by Sarma and colleagues (Sarma et al., 2010) are boxed. Rapsyn residues forming large (>0.40 nm^2) surface of contact with PKA-RIα DD domain homodimer, averaged over the MD trajectory, are underlined. (**B**) Surface of rapsyn residues in contact with PKA-RIα DD domain homodimer. Residues with large contact surface are underlined. (**C**) Cartoon of the complex in water solution as determined by in silico modelling. Rapsyn helix and residues are coloured in red, DD subunits and residues are coloured in brown and silver. Residues forming large contact surface are drawn in balls and sticks and coloured by atom type. In addition, side chains of rapsyn residues are emphasised by a red surface. Inset: Helical wheel diagram of rapsyn amphipathic helix. Residues that form large surface of contact with DD domain homodimer are boxed.

V34 on one partner of the DD domain dimer and residues L13′, Q26′, and K30′ on the opposite side of the DD domain (Fig. 1C). The inset in Fig. 1C shows the rapsyn residues on the helix that face the PKA in boxes.

Rapsyn interacts with PKA type I in cells

On the basis of these findings, we assessed whether rapsyn interacts with PKA type I in cells. To this end we immunoprecipitated rapsyn from lysates of differentiated C2C12 myoblast cells. On western blots, we then confirmed the co-precipitation of PKA-RIα (Fig. 2A). By contrast, α-actinin, a negative control, did not precipitate under these conditions (Fig. 2A). To look at whether the amphipathic helix domain of rapsyn is important for the interaction with PKA-RIα, we performed immunoprecipitation using PKA-RIα-specific antibody on lysates produced from human embryonic kidney cell-derived T-REx293 cells transfected with either full-length rapsyn or rapsyn lacking the amphipathic helix (rapsynΔH, see Fig. 2B for molecular schemes). As depicted in Fig. 2C, full-length rapsyn co-precipitated with PKA-RIα. Conversely, rapsynΔH could not be detected in the precipitate, showing that the amphipathic helix of rapsyn is essential for the interaction with PKA type I.

Next, we studied the interaction of rapsyn with PKA type I by means of bimolecular fluorescence complementation (BiFC) assays (Hu et al., 2002). T-REx293 cells were co-transfected with mCherry as a transfection marker and different combinations of BiFC constructs (see supplementary material Fig. S1 for molecular schemes). In some cases, mCherry was preceded by the RI disruptor peptide RIAD (RIAD-mCherry) (Carlson et al., 2006). In addition to the N- (VN) or C-terminus (VC) of venus protein, BiFC constructs contained either full-length rapsyn and PKA-RIα or truncated versions of these proteins (rapsynΔH and Δdd-PKA-RIα). Two days after transfection, cells were fixed and nuclei stained with draq5. Confocal imaging was used to determine the presence of BiFC (Fig. 3A–D). Quantitative analysis (Fig. 3E) showed that about 40–50% of mCherry-positive cells exhibited punctiform BiFC signals upon co-transfection of full-length rapsyn and PKA-RIα. The amount of BiFC-positive cells significantly dropped to 10–30% in the presence of RIAD-mCherry and the decrease was even more prominent upon coexpression of mutant rapsyn or mutant PKA-RIα. Results were similar irrespective of whether rapsyn and its mutants were present in VC fusions and PKA-RIα and its mutants in VN fusions (Fig. 3E, left half) or in the reverse orientation (Fig. 3E, right half). These results corroborate the immunoprecipitation data and indicate an interaction between rapsyn and PKA-RIα, which relies on the DD domain of PKA-RIα and the α-helical stretch of rapsyn.

In vivo BiFC detects interaction of rapsyn and PKA type I at the NMJ

To verify whether the interaction between rapsyn and PKA-RIα also occurs in vivo and to gauge its localisation, we performed BiFC assays in the muscles of living mice. BiFC constructs were co-transfected in different combinations in mouse tibialis anterior muscles. Ten days later, α-bungarotoxin (BGT), a marker for AChRs, coupled to the fluorescent dye Alexa Fluor 647 (BGT-AF647) was injected to label NMJs. The muscles were then monitored using in vivo imaging. Upon coexpression of rapsyn-VN and PKA-RIα-VC, a high enrichment of BiFC signals was detected in punctiform structures almost exclusively in close proximity to the NMJ (Fig. 4, top row; for low power images see supplementary material Fig. S2). A very similar distribution was

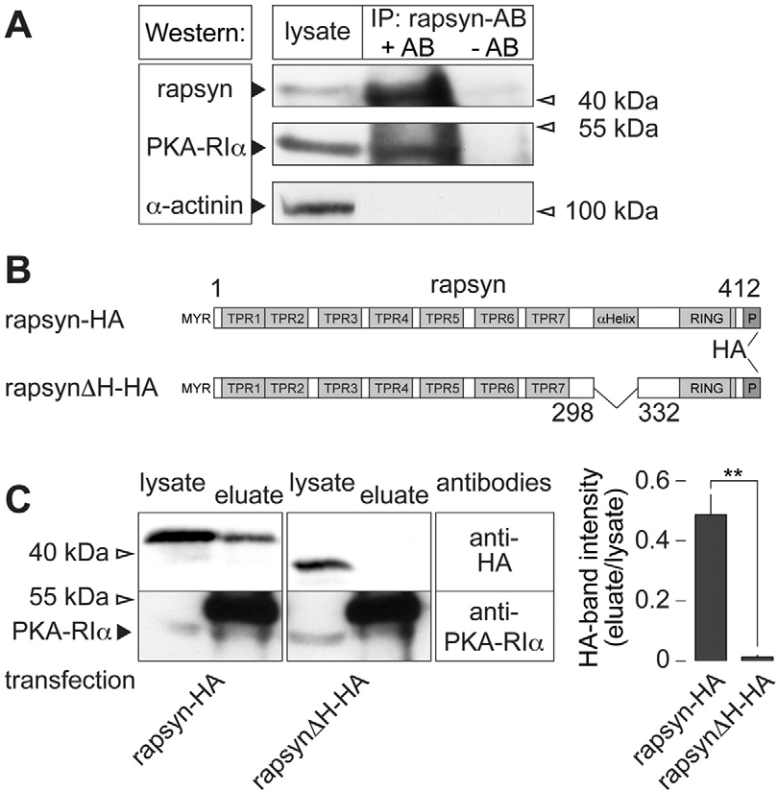

Fig. 2. Rapsyn co-precipitates with PKA-RIα. (**A**) After 10 days of differentiation, C2C12 cells were harvested, and lysates prepared and incubated in the presence or absence of rapsyn antibody (AB). After immunoprecipitation, eluates were run on SDS-PAGE and then probed on western blot using antibodies against rapsyn, PKA-RIα and α-actinin (negative control). The bands show western blot signals in lysates and eluates. (**B**,**C**) T-REx293 cells were transfected with HA-tagged versions of either rapsyn (rapsyn-HA) or a rapsyn mutant lacking the α-helical domain (amino acids 299–331; rapsynΔH-HA). Lysates were prepared, immunoprecipitated with monoclonal anti-PKA-RIα antibody and subsequently probed on western blots for HA and PKA-RIα. (B) Schemes of transfected fusion constructs. (C) Western blot signals in lysates and eluates. Note that only full-length rapsyn co-precipitates with PKA-RIα. The graph on the right shows a densitometric analysis. Depicted are mean ± s.e.m. ($n=3$ experiments) of the eluate band intensities normalised to the lysate. $^{**}P<0.01$ according to Welch test.

shown by coexpression of PKA-RIα-VN and PKA-RIα-VC (Fig. 4, middle row) and was also described previously for full-length PKA-RIα and fluorescent proteins fused to the PKA-RIα DD domain (Barradeau et al., 2001; Röder et al., 2010). Conversely, co-transfection of rapsyn-VN and rapsyn-VC led to the typical rapsyn-like staining, which is almost completely in the NMJ (Fig. 4, bottom row). Strong rapsyn–rapsyn-BiFC signals were expected due to the well-known self-interacting properties of rapsyn (Ramarao et al., 2001; Ramarao and Cohen, 1998).

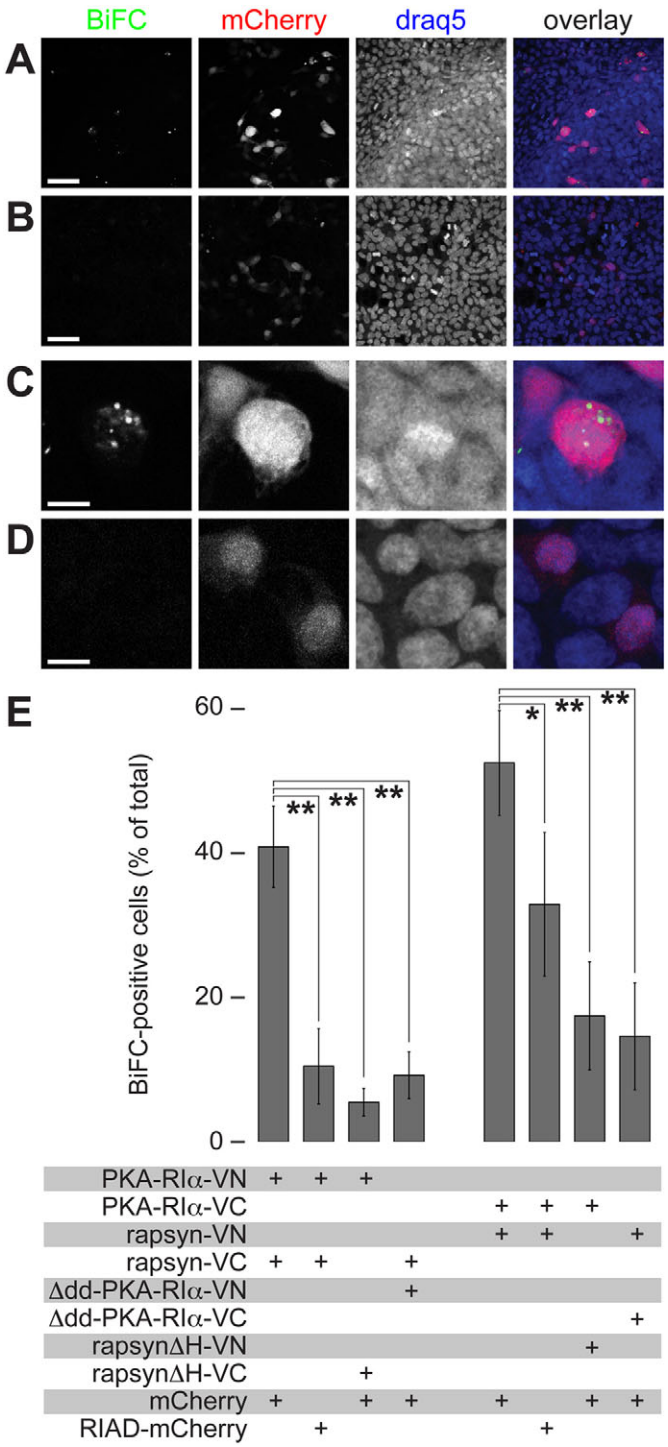

This shows that there is specific interaction between PKA-RIα and rapsyn in close proximity to the NMJ.

Expression of the rapsyn α-helical peptide delocalises PKA type I from its subsynaptic microdomain

Next, we investigated whether the amphipathic helix of rapsyn might function as an AKAP-RI disruptor peptide in vivo. Therefore, a construct expressing this amino acid sequence (rapsyn αHelix) was expressed in the tibialis anterior muscle of live mice. As a control, contra-lateral muscles were transfected with a control peptide in which a number of residues were mutated. Ten days after transfection, muscles were extracted, sliced and the NMJs stained with BGT-AF647. In addition, these slices were immunostained against PKA-RI or rapsyn and then analysed using confocal microscopy (Fig. 5). Notably, although rapsyn staining was equal in controls and rapsyn αHelix-transfected muscles (Fig. 5C,D), PKA-RI staining was clearly reduced in the NMJ region upon expression of the rapsyn αHelix (Fig. 5A,B). Quantitative analysis showed that in controls and rapsyn αHelix-transfected muscles 95.7±0.1% and 97.0±0.7%, respectively, were rapsyn-positive (n=3 different muscles, at least 120 NMJs analysed per condition). For PKA-RI signals, the values were significantly different with 71.9±6.3% and 39.7±8.6% of positive fibres (n=3 different muscles, at least 120 NMJs analysed per condition; P=0.022 according to Welch test). To further consolidate the hypothesis that rapsyn αHelix peptide delocalises PKA-RIα from its subsynaptic site, we used a co-transfection approach (Fig. 5E,F). Muscles were co-transfected with the PKA-RIα localisation marker, RIα-EPAC, and either rapsyn αHelix or the control peptide. Ten days later, NMJs were labelled with BGT-AF647 and then imaged using in vivo confocal microscopy (Fig. 5E). On average, the amount of NMJs exhibiting RIα-EPAC accumulations in the subsynaptic region decreased from 73.4±3.7% (n=4 mice) in the control to 21.4±3.2% (n=4 mice) in the presence of rapsyn αHelix (Fig. 5F). These results strongly indicate that rapsyn is indeed an AKAP targeting PKA-RIα to the NMJ region.

Rapsyn α-helical peptide induces high AChR turnover and synaptic fragmentation

Finally, we asked whether the presence of the rapsyn peptide could mimic the effects of the PKA-RI-specific AKAP disruptor peptide, RIAD (Röder et al., 2010). This was shown to release PKA-RI from its subsynaptic domain and to induce an increased AChR turnover as well as fragmentation of NMJs into numerous separate gutters. Thus, as before, mouse tibialis anterior muscles

Fig. 3. BiFC shows interaction between rapsyn and PKA-RIα. T-REx293 cells were co-transfected with mCherry or RIAD–mCherry and different combinations of BiFC constructs harboring N- (VN) or C-terminals (VC) of Venus and an HA tag together with rapsyn, rapsynΔH, PKA-RIα or Δdd-PKA-RIα (for schemes see supplementary material Fig. S1). Then, cells were fixed, stained with draq5, a nuclear marker, and imaged using confocal microscopy. Subsequently, the fraction of mCherry- or RIAD–mCherry-positive cells showing BiFC signals was determined. (**A**,**B**) Fields of cells co-transfected with PKA-RIα-VN and rapsyn-VC (A) or with PKA-RIα-VN and rapsynΔH-VC (B). Overlays show BiFC signals (green), mCherry signals (red) and nuclei (blue). Scale bars: 50 µm. (**C**,**D**) Blow-ups of regions in A and B. Scale bars: 10 µm. (**E**) Quantification of BiFC-positive cells showing mean ± s.e.m. (n≥3 independent experiments). *P<0.05, **P<0.01 according to Welch test.

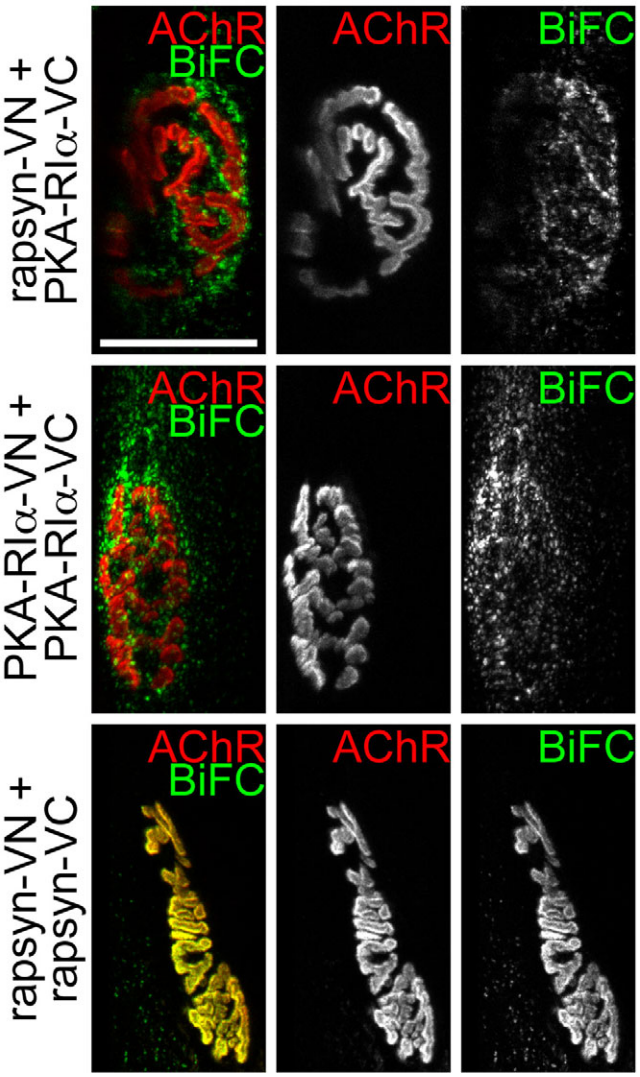

Fig. 4. In vivo BiFC shows interaction between rapsyn and PKA-RIα in a subsynaptic region in live mouse muscle. Mouse tibialis anterior muscles were co-transfected in different combinations as indicated with BiFC constructs harboring N- (VN) or C-terminal (VC-) fragments of Venus protein fused to rapsyn or PKA-RIα. After 10 days, muscles were imaged using in vivo confocal microscopy. NMJs were marked with BGT-AF647. Panels depict maximum *z*-projections of BiFC (green), BGT-AF647 (red) signals and overlays of both (yellow if colocalising) from about 20 confocal slices taken at 1.5 µm interslice interval. Scale bar: 40 µm.

were transfected with rapsyn αHelix and contra-laterally with the control peptide. Simultaneously, AChRs present at this time point were labelled with infrared fluorescent BGT-AF647 (‘old receptors’). Ten days later, red fluorescent BGT-AF555 was applied to mark newly formed AChRs (‘new receptors’). Then, muscles were monitored by in vivo imaging and NMJs were segmented and analysed as described previously (Fig. 6A) (Röder et al., 2010). Notably, in the muscles expressing rapsyn αHelix, the fraction of ‘new receptors’ within the total population of labelled AChRs was highly enriched compared with the control (Fig. 6A). Quantitative analysis revealed values of 0.59 ± 0.13 and 0.06 ± 0.04 for rapsyn αHelix-transfected and control muscles, respectively ($n=6$ muscles and at least 150 NMJs were analysed for each condition; $P<0.01$ according to Welch test) (Fig. 6B). Also, rapsyn αHelix induced significantly more fragmentation of NMJs (supplementary material Fig. S3). On average, 4.2 ± 0.8 and 2.1 ± 0.3 fragments per NMJ were measured in the presence and absence of the rapsyn αHelix, respectively ($n=6$ muscles $P<0.05$ according to Welch test) (Fig. 6B). Together, these data show that binding of PKA to rapsyn is crucial for AChR stability and NMJ integrity and that the rapsyn αHelix peptide reproduces the same phenotype as previously observed upon expression of the PKA-RI-specific AKAP disruptor peptide, RIAD (Röder et al., 2010).

To further substantiate the role of rapsyn in stablising AChRs, we performed two more experiments. First, we tested whether the rapsyn mutant lacking the amphipathic helix (rapsynΔH) would act in a dominant-negative manner. Therefore, tibialis anterior muscles were transfected with this construct and, as before, old and new AChR pools were labelled at a temporal distance of 10 days with BGT-AF647 and BGT-AF555, respectively. Subsequent in vivo imaging (Fig. 6A) and automated quantitative data analysis (Fig. 6B) showed that rapsynΔH was as effective in destabilising AChRs as the rapsyn αHelix peptide (‘new receptor’/total receptor signals, 0.59 ± 0.14, $n=6$ muscles, 210 NMJs analysed). Also the amount of fragments per synapse (5.11 ± 0.46, $n=6$ muscles, 210 NMJs analysed) was increased in a highly significant manner as compared with the control. Second, we used a recently established radiochemical assay (Strack et al., 2011) to determine the AChR half-lives in the presence or absence of rapsyn αHelix peptide. Therefore, 1 week after transfection (left, control; right, αHelix peptide) muscles were pulse-labelled with ^{125}I-BGT. Then, AChR turnover was measured over the next 4 weeks. Although in both sides AChRs displayed the typical two-term lifetime distribution with a short-lived (half-life, $t_{1/2}$ 1.1 days) and a long-lived population of receptors, AChR lifetime was clearly affected in the rapsyn αHelix peptide-expressing muscles (Fig. 6C). In particular, the short-lived receptors pool increased from $17.2\pm3.1\%$ ($n=5$ mice) in the control to $35.3\pm2.8\%$ ($n=5$ mice) in the rapsyn αHelix-expressing muscles. These data corroborate the imaging data and clearly indicate that the rapsyn αHelix peptide strongly impacts on AChR lifetime.

Discussion

Rapsyn is known to be important for the formation and maintenance of the vertebrate NMJ (Gautam et al., 1995). There is a wealth of studies showing a direct correlation between the amount of rapsyn present at NMJs and the abundance or the metabolic stability of synaptic AChRs (Brockhausen et al., 2008; Gervasio et al., 2007; Gervasio and Phillips, 2005; Luo et al., 2008; Martinez-Martinez et al., 2009; Wang et al., 1999). Furthermore, mutations in the RAPSN gene are amongst the most frequent causes for myasthenic syndromes, which are characterised by activity-dependent muscle weakness (Beeson et al., 2008; Müller et al., 2007). Together, these findings place rapsyn in the centre of regulatory processes that mediate stabilisation of synaptic AChRs.

Given previous reports highlighting a role of cAMP and PKA type I in AChR stabilisation (Nelson et al., 2003; Shyng et al., 1991; Xu and Salpeter, 1997) and in the light of our previous finding that a complex of recycling AChRs, myosin Va, and PKA-RI is crucial for the stabilisation of AChRs (Röder et al., 2010), it was important to establish which protein links PKA type

I to the subsynaptic microdomain. Prime players in targeting PKA molecules to subcellular sites are AKAPs, and one of their hallmark features is a PKA-R-interacting amphipathic α-helical stretch (Colledge and Scott, 1999). Owing to the presence of such a domain, its described role in AChR stabilisation and its molecular interaction with AChRs, rapsyn appears to be an ideal candidate for mediating the anchoring of PKA-RI close to the NMJ. In this study we provide biochemical, in vitro, in silico and in vivo data that strongly support the role of rapsyn as the AKAP that mediates accumulation of PKA type I close to the NMJ,

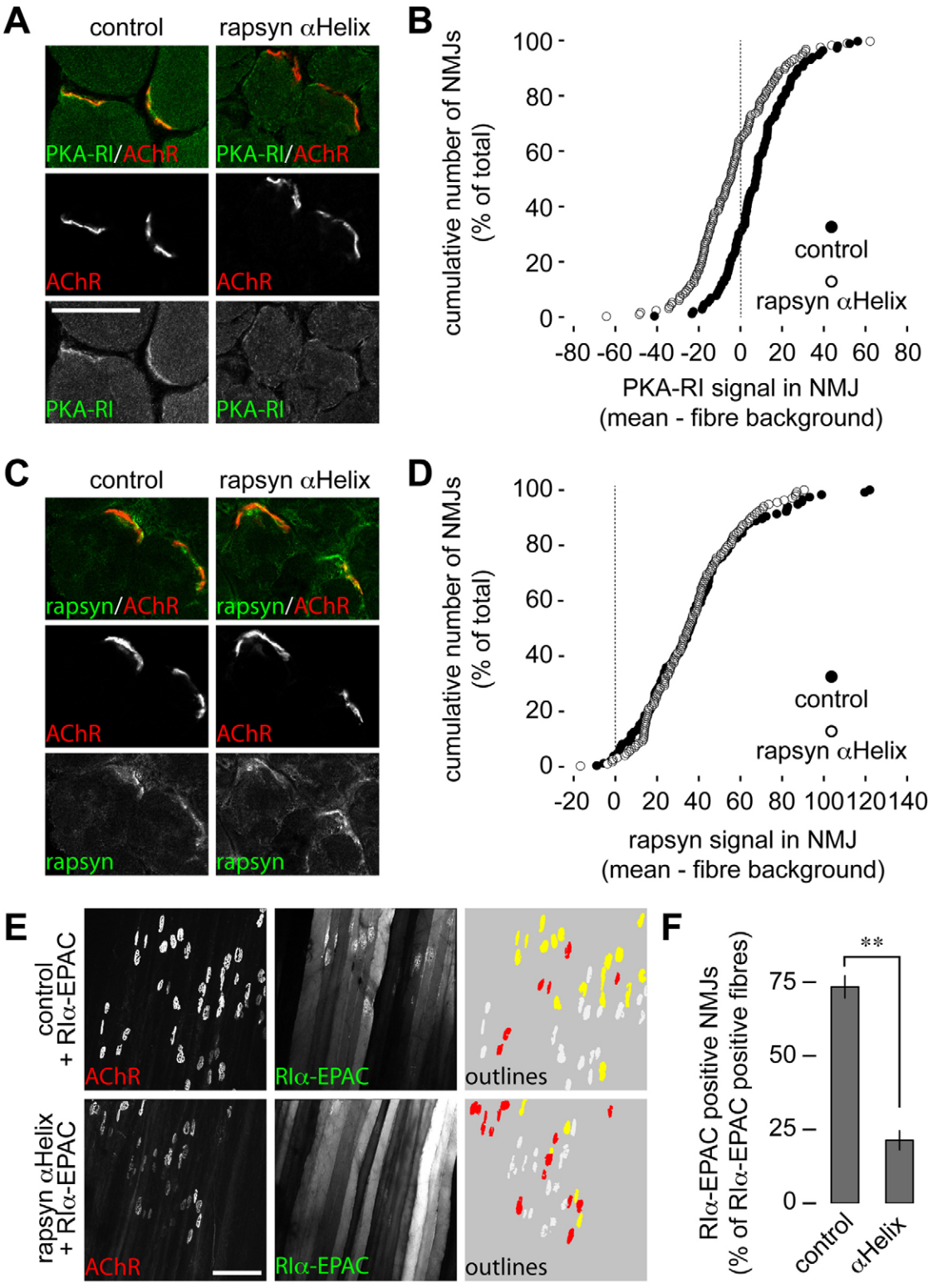

Fig. 5. See next page for legend.

which in turn is a pre-requisite for proper stabilisation of synaptic AChRs.

We first compared rapsyn amphipathic helix (Ramarao et al., 2001) to a sequence alignment of 22 known AKAP-binding proteins (McLaughlin et al., 2011), which includes also AKAP10. The structure of AKAP10 amphipathic helix in complex with PKA-RIα was recently solved (Sarma et al., 2010) and was used here as template to model the rapsyn–PKA-RIα complex. We found that the AKAP10 residues that occupy the four main interaction pockets as defined by Sarma and colleagues (Sarma et al., 2010) are substituted in rapsyn by similar hydrophobic residues, except for K311 and S324. These two residues are partially solvent-exposed and the corresponding alignment positions are not conserved. However, K311 aligns with lysine from AKAP12 and MTG16, and S324 aligns with other polar residues (Fig. 1A). Besides the residues from the four interaction pockets, A308 and K327 from the N- and C-termini of the helix, respectively, were found to contribute to the binding stability by forming additional contacts with the PKA-RIα DD domain homodimer (Fig. 1C). The network of interprotein interactions overlaps with the AKAP10–PKA-RIα interaction pattern observed in the X-ray structure of the complex (Sarma et al., 2010) and suggests that rapsyn interaction with PKA-RIα is mostly non-polar. Nevertheless, we cannot exclude the possibility that regions at the N-terminal of the rapsyn amphipathic helix (not included in our model) could enhance targeting to PKA-RIα by forming additional interactions, as proposed for dual-specificity AKAPs (Jarnaess et al., 2008).

Biochemical pull-down (Fig. 2) and BiFC experiments (Fig. 3) obtained in C2C12 and T-REx293 cells corroborate the modelling data and show that PKA type I and rapsyn interact with each other by binding of the PKA-RI DD domain to the rapsyn α-helical domain. In vivo BiFC, using PKA-RIα and rapsyn as interaction partners showed a strong enrichment of BiFC signals in punctiform structures close to the NMJ but not within the NMJ (Fig. 4). Notably, no or very few BiFC signals were detected only a few micrometers away from the NMJ (supplementary material Fig. S2). This pattern was very similar to that of PKA-RIα and PKA-RIα-BiFC signals. Conversely, rapsyn–rapsyn BiFC signals almost perfectly matched the NMJ staining and showed only few punctuate structures. To explain the discrepancy between the distributions of the rapsyn–PKA BiFC and the rapsyn–rapsyn BiFC, it is important to consider two main factors: first, a small pool of rapsyn is known to be constantly present in intracellular, vesicular compartments although it is primarily found in the NMJ (Bruneau and Akaaboune, 2010; Gervasio and Phillips, 2005). Second, BiFC between two interaction partners occurs at their site of contact (Hu and Kerppola, 2003) and therefore indicates the location of interaction rather than the steady-state distribution of both proteins. Based on our findings and the general aspects of rapsyn and BiFC as just mentioned, we speculate that rapsyn interacts with PKA-RIα in a domain close to the NMJ. As shown recently, the accumulation of PKA-RIα in this region is crucial for proper AChR stabilisation (Röder et al., 2010; Röder et al., 2008; Yampolsky et al., 2010a).

In previous reports, the rapsyn α-helical domain was described as mediating AChR clustering at the surface of human embryonic kidney cells coexpressing different rapsyn mutants plus all AChR subunits (Ramarao et al., 2001; Ramarao and Cohen, 1998). Essentially, in these studies BGT-positive patches on the cell surface were present or absent upon coexpression of wild-type rapsyn or rapsyn lacking the α-helical domain, respectively. Although these results nicely showed the importance of the α-helical domain for AChR surface exposure, it remained unclear how rapsyn mediates this process. Although our study does not rule out a direct AChR clustering effect of the rapsyn α-helical domain, one might also envisage an indirect mechanism by which rapsyn, acting as an AKAP, might enhance PKA-dependent effector phosphorylation and enable subsequent AChR clustering. Because the mechanisms of AChR clustering and stabilisation are still elusive, this question has to remain open for the moment.

We designed peptides mimicking the rapsyn α-helical domain to test their functional effect as potential AKAP disruptor peptides in the living mouse. These peptides, but not mutated control peptides, efficiently delocalised PKA-RI from the NMJ (Fig. 5) and induced significant alterations in AChR turnover and NMJ morphology (Fig. 6). These effects remarkably resembled those induced by the PKA-RI-specific AKAP-disruptor peptide, RIAD (Carlson et al., 2006), on the same parameters in mouse NMJs (Röder et al., 2010). Overexpression of a rapsyn deletion mutant lacking the amphipathic helix had a similar effect on AChR turnover and NMJ morphology, which strongly suggests that rapsyn is an AKAP for PKA type I in the NMJ and further corroborates the important role of cAMP–PKA-dependent signalling in regulating AChR turnover and NMJ morphology. In extension to our previous model, a small pool of extrasynaptic rapsyn might therefore anchor PKA-RIα to the AChR recycling compartment. Our data also fit the observation of a high turnover rate of rapsyn at the NMJ (Bruneau and Akaaboune, 2010), because our model would benefit from a reversible and non-permanent interaction between rapsyn and AChR.

We envisage that rapsyn recycles with AChRs by some kind of membrane transport. During its presence in a putative recycling compartment, some post-translational modification of rapsyn might enable its transient binding of PKA-RIα. This would allow

Fig. 5. Peptide encompassing rapsyn α-helical domain displaces PKA-RIα from its subsynaptic microdomain in vivo. (**A**–**F**) A peptide encompassing the rapsyn α-helix (rapsyn αHelix) or a mutant control peptide (control) was transfected (A–D) or co-transfected together with RIα-EPAC (E,F), a marker for the localisation of PKA-RIα, into mouse tibialis anterior muscles. After 10 days, muscles were extracted, sliced and stained against AChR with BGT-AF647, and with antibodies against PKA-RI (A,B) or rapsyn (C,D), or injected with BGT-AF647 and then imaged in vivo (E,F). Stained sections were analysed with confocal microscopy, and antibody staining intensities in the NMJs were determined (see Materials and Methods section for details). (A,C) Confocal slices of muscles transfected as indicated. In overlays, antibody signals are shown in green, BGT signals in red. Scale bar: 50 μm. (B,D) Cumulative plots showing the antibody staining intensities in all analysed NMJs. All NMJs right of the zero value (dotted line) were counted as PKA-RI- or rapsyn-positive. (E) Images depict maximum *z*-projections of 80 (upper panels) and 97 optical slices (lower panels) taken at 3 μm interslice intervals of muscles co-transfected as indicated on the left. Images show BGT (AChR), RIα-EPAC fluorescence signals or pseudo-coloured NMJ outlines. In the outlines: NMJs in white, synapses of RIα-EPAC-negative fibres; NMJs in yellow, synapses of RIα-EPAC-positive fibres with subsynaptic RIα-EPAC accumulations; NMJs in red, synapses of RIα-EPAC-positive fibres without subsynaptic RIα-EPAC accumulations. Scale bar: 200 μm. (F) Quantitative analysis showing the average amount (mean ± s.e.m.) of NMJs of RIα-EPAC-positive fibres with subsynaptic RIα-EPAC accumulations. $n=4$ mice; 382 NMJs (control) and 425 NMJs (αHelix) were analysed. $^{**}P<0.01$ according to Welch test.

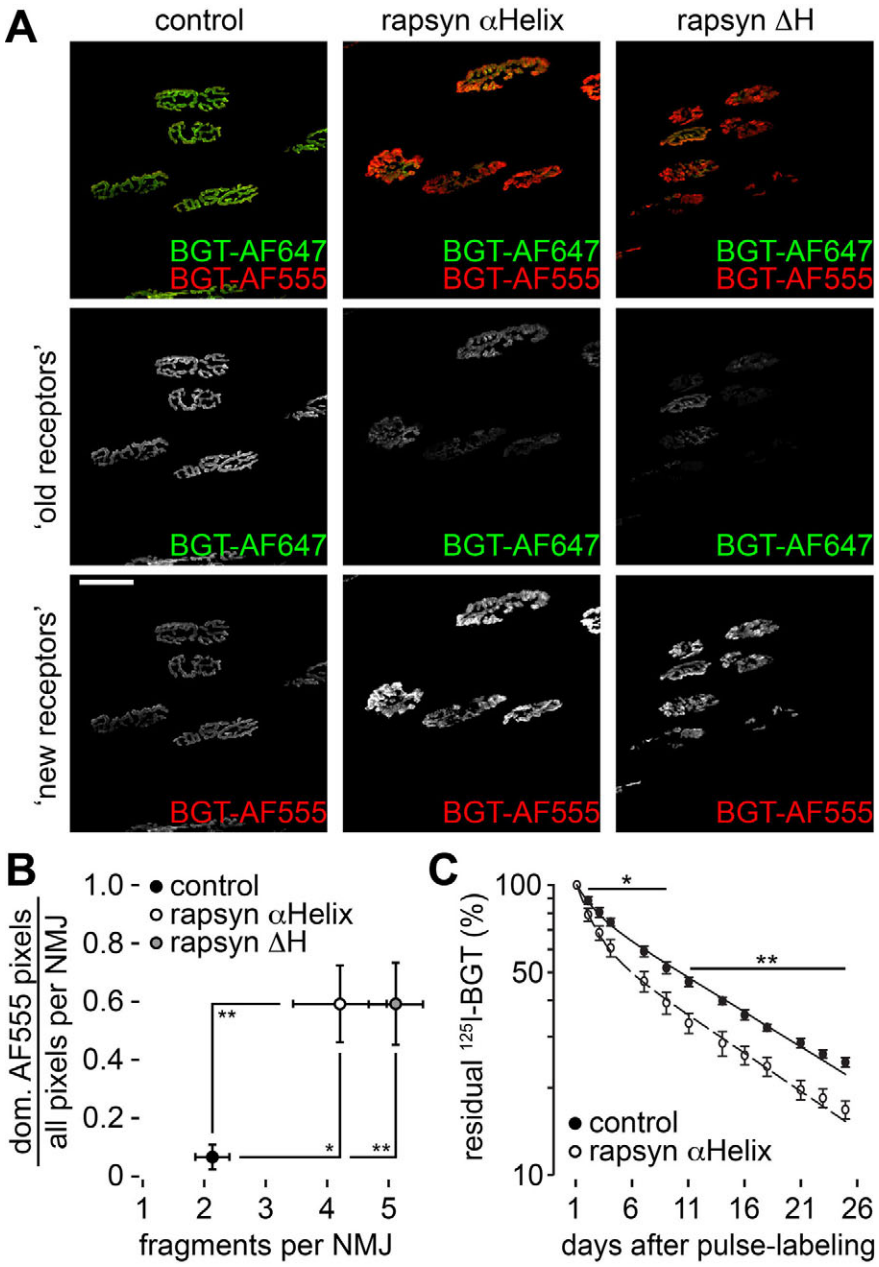

Fig. 6. Peptide encompassing rapsyn α-helical domain and rapsyn-ΔHelix alter AChR turnover and fragmentation of NMJs in live mouse muscle. (**A**,**B**) A peptide encompassing the rapsyn α-helix (rapsyn αHelix), a mutant control peptide (control) or rapsyn-ΔHelix was transfected into mouse tibialis anterior muscles. AChRs present on the cell surface at the time point of transfection were labelled by locally injected BGT-AF647 ('old receptors'). After 10 days, muscles were injected with BGT-AF555 to mark AChRs now available ('new receptors'). Then, muscles were imaged by in vivo confocal microscopy and automatically segmented and analysed. (A) Maximum *z*-projections of automatically segmented confocal slices taken at an interslice interval of 1.5 µm. In overlays, 'old receptors' are shown in green and 'new receptors' in red. Scale bar: 50 µm. (B) Quantitative analysis of AChR turnover and NMJ fragmentation. Shown are average values (mean ± s.e.m.) of the fractions of all pixels in NMJs with dominant 'new receptor' signals as a function of the numbers of fragments per NMJ ($n=6$ muscles). (**C**) Seven days after transfection, muscles were injected with ^{125}I-BGT to pulse-label AChRs. Then, residual ^{125}I-activity was measured at depicted time intervals. The time point of pulse labelling is t_0. The graph shows the residual ^{125}I-emission in the injected hindlimbs as a function of time after pulse labelling. Dots represent measured values (mean ± s.e.m., $n=5$ mice) and lines indicate two-term exponential fits. Data are normalised to the mean values measured on day 1. $^*P<0.05$, $^{**}P<0.01$ according to Welch test.

enrichment of PKA-RIα close to the NMJ. Upon arrival of an appropriate local cAMP stimulus, PKA-RIα might then phosphorylate effector proteins leading to the stabilisation of synaptic AChRs. It remains a major future task to unravel how such receptor stabilisation is mechanistically performed.

Materials and Methods

Chemicals, antibodies and cDNAs

Primary antibodies were purchased against α-actinin (Sigma-Aldrich, Hamburg, Germany), haemagglutinin (HA; Sigma-Aldrich), GAPDH (Santa Cruz Biotechnology, Heidelberg, Germany), PKA-RIα (BD Bioscience, Heidelberg, Germany) and rapsyn (Lifespan Bioscience, Seattle, WA), and secondary antibodies conjugated to horseradish peroxidase (Dako, Hamburg, Germany), Alexa Fluor 488 or Alexa Fluor 546 (Invitrogen, Darmstadt, Germany). BGT-AF555 and BGT-AF647 were from Invitrogen. Rapsyn-HA and ΔH-rapsyn-HA vector constructs for co-precipitation used wild-type (1,236 bps, 412 amino acids) and a α-helical coiled-coil domain deletion mutant (deleted sequence: bps 892–996 corresponding to amino acids 298–332) of rapsyn cDNAs. They were amplified by PCR from a rapsyn–GFP expression vector (Jonathan Cohen, Harvard Medical School, Boston, MA) with primers containing a C-terminal HA tag and were then subcloned into *Bam*HI and *Eco*RI cleaved pcDNA3.1(+) (Invitrogen). For BiFC, wild-type (1,143 bps, 381 amino acids) and a DD domain deletion mutant (Δdd-PKA-RIα; lacking bps 1–186 corresponding to amino acids 1–62) of PKA-RIα cDNAs were amplified by PCR from PKA-RIα expression vector. Wild-type and ΔH-mutant of rapsyn (without HA tag) were prepared as described above. Amplified cDNAs were cloned into pBiFC-VN or pBiFC-VC vectors containing a HA tag as described (Röder et al., 2010). The amino acid sequence GSGGGGGSG was used as a linker between target molecule and Venus fragment. HA tags were positioned at N- and C-terminal of rapsyn and PKA-RIα, respectively. For functional studies, the cDNA sequences of wild-type (rapsyn αHelix; amino acids 280–331) and mutant (rapsyn αHelix mut; N281, G284, Q285, H287, V288, L289, L306, I309, Q313, E317 substituted to alanine) α-helical coiled-coil domain of rapsyn were amplified by PCR and cloned into *Eco*RI and *Xho*I cleaved pcDNA3.1(+) (Invitrogen).

Cells, animals and transfection

For culture cell transfection, T-REx293 cells (Invitrogen) were seeded on 10-cm petri-dishes (Greiner Bio-One, Frickenhausen, Germany) and cultured in 10% FBS

DMEM at 37℃ with 5% CO_2. 4 µg of each vector construct were transfected using 10 µl Lipofectamine 2000 (Invitrogen) in DMEM without FBS for 24 hours. Then, medium was changed to normal FBS-containing medium for 1 day and cells were prepared for further analysis. C2C12 cells (ATCC, Wesel, Germany) were cultured in the same way as T-Rex293 cells. For differentiation, C2C12 cells were switched at 70% of confluency to medium containing 2% FBS instead of horse serum. C57BL/6J mice were used for in vivo BiFC and functional studies. Animals were from Charles River (Sulzfeld, Germany) and then maintained in the local animal facility. Use and care of animals was as approved by German authorities and according to national law (TierSchG§7). An intraperitoneal injection of Rompun (Bayer, Leverkusen, Germany) and Zoletil 100 (Laboratoires Virbac, Carros Cedex, France) was used for anesthesia. Transfection was carried out as previously described (Dona et al., 2003; Röder et al., 2010).

Immunoprecipitation

After transfection, cells were washed twice with PBS and collected in the presence of 500 µl lysis buffer (50 mM Tris-Cl pH 8.9, 150 mM NaCl, 1% NP-40, 10% glycerol, 1 mM EDTA, 1 mM EGTA, 2 mM Na_3VO_4, 1 mM NaF, 0.5 mM PMSF, 1 mM DTT, 10 mM glycerol phosphate and Complete Protease inhibitor cocktail). After 30 minutes at 4℃ with gentle rocking, lysates were centrifuged at 13,000 ***g*** for 20 minutes and supernatants were incubated with PKA-RIα monoclonal or rapsyn polyclonal antibody at 4℃ in a rotating wheel for overnight. Then, 50 µl of protein A and protein G agarose mixture (Calbiochem, Darmstadt, Germany) was added and incubated at 4℃ for 2 hours. Finally, samples were centrifuged for 1 minute at 500 ***g***, washed three times with lysis buffer and eluted by Laemmli buffer for SDS-PAGE and western blot. For SDS-PAGE, protein concentrations of every sample were measured using Bradford solution (BioRad, München, Germany) and further steps were as described (Rudolf et al., 2003).

Cell and tissue staining

After transfection, cells were washed twice with PBS and fixed in 4% paraformaldehyde at room temperature for 10 minutes. Fixed cells were permeabilised with 0.1% Triton X-100 at room temperature for 10 minutes and then quenched with 50 mM NH_4Cl. Between each step, cells were washed with PBS. Blocking was carried out by incubation at room temperature for 1 hour with 10% FBS containing PBS and primary antibody. After washing with PBS, secondary antibodies and draq5 were added and incubation continued at room temperature for 1 hour. Finally, cells were washed with PBS and distilled water and mounted on glass slides with Mowiol. Muscle slicing and immunostaining was as described (Röder et al., 2010).

Microscopy and AChR lifetime measurements

Imaging and image analysis of live mouse muscles was as described (Röder et al., 2010). For BiFC experiments using culture cells, images were taken with a DMRE TCS SP2 confocal microscope equipped with Leica Confocal Software 2.61, a KrAr laser (488 nm), a diode-pumped laser (561 nm), a HeNe laser (633 nm), and a 63×, 1.4 NA HCX PL APO CS oil immersion objective (Leica Microsystems, Mannheim, Germany). Fluorescence signals of Venus, mCherry (or AF546) and draq5 were excited at 488, 561 and 633 nm, and emission was detected using band-pass settings of 500–550 nm, 570–620 nm, and 650–750 nm, respectively. 3D image stacks were taken at 12-bit and 1024-pixel resolution with 1× or 4× zoom, 200 Hz scan frequency and 2× line average. ^{125}I-BGT-based determination of AChR turnover was as described (Strack et al., 2011) with the exception that only about 700 fmol of ^{125}I-BGT was applied per leg.

Computational methods

The profile Hidden Markov model (HMM) of the PKA binding motif of AKAPs was calculated from AKAP sequence alignment (McLaughlin et al., 2011) and aligned with the rapsyn fragment using the program HMMER v.3.0 (www.hmmer.org). The structural model of the complex between PKA-RIα DD domains and rapsyn was based on the X-ray structure of the complex between PKA-RIα DD domains and the AKAP10 amphipatic helix solved at resolution 2.29 Å (AKAP10 fragment 628–654, PDB entry code 3IM4) (Sarma et al., 2010). AKAP10 was replaced by rapsyn fragment 305–331 on the basis of the alignment in Fig. 1A, to end up with the structural model of the complex between PKA-RIα DD domains and rapsyn amphipathic helix. The MODELLER program was used to model the complex (Eswar et al., 2007). Hydrogen atoms were added by assuming standard bond lengths and angles. The model was immersed in a parallelepiped box whose edges were 8.3, 8.3 and 8.1 nm, containing 17,765 water molecules; three sodium ions were added to neutralise the box. The computational setup was as described (Berrera et al., 2006b). After energy minimisation and 60 picoseconds of solvent equilibration, the complex underwent 100 nanoseconds of molecular dynamics in the isothermal-isobaric ensemble at 300°K and 1 atm. The minimum distance between periodic images of the complex in solution turned out to be always as large as 3.0 nm. Contact surface, H-bonds and RMSD were calculated as described (Berrera et al., 2006a).

Data analysis and statistics

Image analysis was done using the ImageJ program (NIH, Bethesda, MD) or as described (Röder et al., 2010). Automated NMJ segmentation as used in Fig. 6 and analysis of AChR turnover and synapse fragmentation were as described [see figure S5 in Röder et al. (Röder et al., 2010)]. For cellular BiFC analysis, maximum *z*-projections of each channel were median-filtered (1 pixel kernel) and background fluorescence was subtracted. Cells were counted as BiFC-positive if they exhibited more than 10 pixels above background in the Venus channel. Stained muscle slices were analysed as follows: first, regions of interest (ROIs) containing the NMJ area were determined using thresholding of the BGT-AF647-positive areas. Then, fibre ROIs containing the entire fibre excluding the NMJ ROIs were created manually. Mean signal intensities and standard deviations of PKA-RI or rapsyn antibody staining signals were measured in NMJ and fibre ROIs. Cumulative plots show the sorted list of values from mean antibody signals in the NMJ region subtracted by the mean signal plus standard deviation in the fibre ROIs. Each data point represents one analysed NMJ. All data were tested for normality using the Kolmogorow–Smirnow–Lilliefors test. Homo- and heteroscedasticity was evaluated using the *F*-test. Significance was tested using either the Student's *t*-test or Welch test, as applicable. Values given are mean ± s.e.m., unless otherwise stated. Data calculations, statistical analyses and figure preparation used Microsoft Excel (Unterschleissheim, Germany), SigmaPlot (San Jose, CA), Adobe Photoshop, and Adobe Illustrator (San Jose, CA) software.

Acknowledgements

We are grateful to Jonathan Cohen (Boston, MA), Olivier Kassel (Karlsruhe, Germany) and Veit Witzemann (Heidelberg, Germany) for generous gifts of constructs. We thank the animal facility of ITG for their excellent support and Christoph Wilhelm and Susanne Kaminski (Karlsruhe, Germany) for help with the AChR lifetime determination.

Funding

R.R. was supported by the Deutsche Forschungsgemeinschaft [grant number RU923/3-1] and Association Française contre les Myopathies [grant number 12056].

Supplementary material available online at
http://jcs.biologists.org/lookup/suppl/doi:10.1242/jcs.092361/-/DC1

References

Akaaboune, M., Culican, S. M., Turney, S. G. and Lichtman, J. W. (1999). Rapid and reversible effects of activity on acetylcholine receptor density at the neuromuscular junction in vivo. *Science* **286**, 503-507.

Barradeau, S., Imaizumi-Scherrer, T., Weiss, M. C. and Faust, D. M. (2001). Muscle-regulated expression and determinants for neuromuscular junctional localization of the mouse RIalpha regulatory subunit of cAMP-dependent protein kinase. *Proc. Natl. Acad. Sci. USA* **98**, 5037-5042.

Beeson, D., Webster, R., Cossins, J., Lashley, D., Spearman, H., Maxwell, S., Slater, C. R., Newsom-Davis, J., Palace, J. and Vincent, A. (2008). Congenital myasthenic syndromes and the formation of the neuromuscular junction. *Ann. N. Y. Acad. Sci.* **1132**, 99-103.

Berrera, M., Cattaneo, A. and Carloni, P. (2006a). Molecular simulation of the binding of nerve growth factor peptide mimics to the receptor tyrosine kinase A. *Biophys. J.* **91**, 2063-2071.

Berrera, M., Pantano, S. and Carloni, P. (2006b). cAMP Modulation of the cytoplasmic domain in the HCN2 channel investigated by molecular simulations. *Biophys. J.* **90**, 3428-3433.

Brockhausen, J., Cole, R. N., Gervasio, O. L., Ngo, S. T., Noakes, P. G. and Phillips, W. D. (2008). Neural agrin increases postsynaptic ACh receptor packing by elevating rapsyn protein at the mouse neuromuscular synapse. *Dev. Neurobiol.* **68**, 1153-1169.

Bruneau, E. G. and Akaaboune, M. (2010). Dynamics of the rapsyn scaffolding protein at the neuromuscular junction of live mice. *J. Neurosci.* **30**, 614-619.

Bruneau, E., Sutter, D., Hume, R. I. and Akaaboune, M. (2005). Identification of nicotinic acetylcholine receptor recycling and its role in maintaining receptor density at the neuromuscular junction in vivo. *J. Neurosci.* **25**, 9949-9959.

Carlson, C. R., Lygren, B., Berge, T., Hoshi, N., Wong, W., Tasken, K. and Scott, J. D. (2006). Delineation of type I protein kinase A-selective signaling events using an RI anchoring disruptor. *J. Biol. Chem.* **281**, 21535-21545.

Colledge, M. and Scott, J. D. (1999). AKAPs: from structure to function. *Trends Cell Biol.* **9**, 216-221.

Dona, M., Sandri, M., Rossini, K., Dell'Aica, I., Podhorska-Okolow, M. and Carraro, U. (2003). Functional in vivo gene transfer into the myofibers of adult skeletal muscle. *Biochem. Biophys. Res. Commun.* **312**, 1132-1138.

Eswar, N., Webb, B., Marti-Renom, M. A., Madhusudhan, M. S., Eramian, D., Shen, M. Y., Pieper, U. and Sali, A. (2007). Comparative protein structure modeling using MODELLER. *Curr. Protoc. Protein Sci.* **50**, 2.9.1-2.9.31.

Fambrough, D. M. (1979). Control of acetylcholine receptors in skeletal muscle. *Physiol. Rev.* **59**, 165-227.

Frail, D. E., McLaughlin, L. L., Mudd, J. and Merlie, J. P. (1988). Identification of the mouse muscle 43,000-dalton acetylcholine receptor-associated protein (RAPsyn) by cDNA cloning. *J. Biol. Chem.* **263**, 15602-15607.

Gautam, M., Noakes, P. G., Mudd, J., Nichol, M., Chu, G. C., Sanes, J. R. and Merlie, J. P. (1995). Failure of postsynaptic specialization to develop at neuromuscular junctions of rapsyn-deficient mice. *Nature* **377**, 232-236.

Gervasio, O. L. and Phillips, W. D. (2005). Increased ratio of rapsyn to ACh receptor stabilizes postsynaptic receptors at the mouse neuromuscular synapse. *J. Physiol.* **562**, 673-685.

Gervasio, O. L., Armson, P. F. and Phillips, W. D. (2007). Developmental increase in the amount of rapsyn per acetylcholine receptor promotes postsynaptic receptor packing and stability. *Dev. Biol.* **305**, 262-275.

Hu, C. D. and Kerppola, T. K. (2003). Simultaneous visualization of multiple protein interactions in living cells using multicolor fluorescence complementation analysis. *Nat. Biotechnol.* **21**, 539-545.

Hu, C. D., Chinenov, Y. and Kerppola, T. K. (2002). Visualization of interactions among bZIP and Rel family proteins in living cells using bimolecular fluorescence complementation. *Mol. Cell* **9**, 789-798.

Jarnaess, E., Ruppelt, A., Stokka, A. J., Lygren, B., Scott, J. D. and Tasken, K. (2008). Dual specificity A-kinase anchoring proteins (AKAPs) contain an additional binding region that enhances targeting of protein kinase A type I. *J. Biol. Chem.* **283**, 33708-33718.

Lomo, T. and Rosenthal, J. (1972). Control of ACh sensitivity by muscle activity in the rat. *J. Physiol.* **221**, 493-513.

Luo, S., Zhang, B., Dong, X. P., Tao, Y., Ting, A., Zhou, Z., Meixiong, J., Luo, J., Chiu, F. C., Xiong, W. C. et al. (2008). HSP90 beta regulates rapsyn turnover and subsequent AChR cluster formation and maintenance. *Neuron* **60**, 97-110.

Martinez-Martinez, P., Phernambucq, M., Steinbusch, L., Schaeffer, L., Berrih-Aknin, S., Duimel, H., Frederik, P., Molenaar, P., De Baets, M. H. and Losen, M. (2009). Silencing rapsyn in vivo decreases acetylcholine receptors and augments sodium channels and secondary postsynaptic membrane folding. *Neurobiol. Dis.* **35**, 14-23.

McLaughlin, W. A., Hou, T., Taylor, S. S. and Wang, W. (2011). The identification of novel cyclic AMP-dependent protein kinase anchoring proteins using bioinformatic filters and peptide arrays. *Protein Eng. Des. Sel.* **24**, 333-339.

Müller, J. S., Mihaylova, V., Abicht, A. and Lochmüller, H. (2007). Congenital myasthenic syndromes: spotlight on genetic defects of neuromuscular transmission. *Expert Rev. Mol. Med.* **9**, 1-20.

Nelson, P. G., Lanuza, M. A., Jia, M., Li, M. X. and Tomas, J. (2003). Phosphorylation reactions in activity-dependent synapse modification at the neuromuscular junction during development. *J. Neurocytol.* **32**, 803-816.

Ramarao, M. K. and Cohen, J. B. (1998). Mechanism of nicotinic acetylcholine receptor cluster formation by rapsyn. *Proc. Natl. Acad. Sci. USA* **95**, 4007-4012.

Ramarao, M. K., Bianchetta, M. J., Lanken, J. and Cohen, J. B. (2001). Role of rapsyn tetratricopeptide repeat and coiled-coil domains in self-association and nicotinic acetylcholine receptor clustering. *J. Biol. Chem.* **276**, 7475-7483.

Röder, I. V., Petersen, Y., Choi, K. R., Witzemann, V., Hammer, J. A., 3rd and Rudolf, R. (2008). Role of myosin Va in the plasticity of the vertebrate neuromuscular junction in vivo. *PLoS ONE* **3**, e3871.

Röder, I. V., Choi, K. R., Reischl, M., Petersen, Y., Diefenbacher, M. E., Zaccolo, M., Pozzan, T. and Rudolf, R. (2010). Myosin Va cooperates with PKA RIalpha to mediate maintenance of the endplate in vivo. *Proc. Natl. Acad. Sci. USA* **107**, 2031-2036.

Rudolf, R., Kögel, T., Kuznetsov, S. A., Salm, T., Schlicker, O., Hellwig, A., Hammer, J. A., 3rd and Gerdes, H. H. (2003). Myosin Va facilitates the distribution of secretory granules in the F-actin rich cortex of PC12 cells. *J. Cell Sci.* **116**, 1339-1348.

Rudolf, R., Bittins, C. M. and Gerdes, H. H. (2011). The role of myosin V in exocytosis and synaptic plasticity. *J. Neurochem.* **116**, 177-191.

Sarma, G. N., Kinderman, F. S., Kim, C., von Daake, S., Chen, L., Wang, B. C. and Taylor, S. S. (2010). Structure of D-AKAP2:PKA RI complex: insights into AKAP specificity and selectivity. *Structure* **18**, 155-166.

Shyng, S. L., Xu, R. and Salpeter, M. M. (1991). Cyclic AMP stabilizes the degradation of original junctional acetylcholine receptors in denervated muscle. *Neuron* **6**, 469-475.

Stanley, E. F. and Drachman, D. B. (1981). Denervation accelerates the degradation of junctional acetylcholine receptors. *Exp. Neurol.* **73**, 390-396.

Strack, S., Petersen, Y., Wagner, A., Röder, I. V., Albrizio, M., Reischl, M., Wacker, I. U., Wilhelm, C. and Rudolf, R. (2011). A novel labeling approach identifies three stability levels of acetylcholine receptors in the mouse neuromuscular junction in vivo. *PLoS ONE* **6**, e20524.

Wang, Z. Z., Mathias, A., Gautam, M. and Hall, Z. W. (1999). Metabolic stabilization of muscle nicotinic acetylcholine receptor by rapsyn. *J. Neurosci.* **19**, 1998-2007.

Witzemann, V., Barg, B., Nishikawa, Y., Sakmann, B. and Numa, S. (1987). Differential regulation of muscle acetylcholine receptor gamma- and epsilon-subunit mRNAs. *FEBS Lett.* **223**, 104-112.

Xu, R. and Salpeter, M. M. (1997). Acetylcholine receptors in innervated muscles of dystrophic mdx mice degrade as after denervation. *J. Neurosci.* **17**, 8194-8200.

Xu, R. and Salpeter, M. M. (1999). Rate constants of acetylcholine receptor internalization and degradation in mouse muscles. *J. Cell. Physiol.* **181**, 107-112.

Yampolsky, P., Pacifici, P. G., Lomb, L., Giese, G., Rudolf, R., Röder, I. V. and Witzemann, V. (2010a). Time lapse in vivo visualization of developmental stabilization of synaptic receptors at Neuromuscular Junctions. *J. Biol. Chem.* **285**, 34589-34596.

Yampolsky, P., Pacifici, P. G. and Witzemann, V. (2010b). Differential muscle-driven synaptic remodeling in the neuromuscular junction after denervation. *Eur. J. Neurosci.* **31**, 646-658.

Zaccolo, M. (2009). cAMP signal transduction in the heart: understanding spatial control for the development of novel therapeutic strategies. *Br. J. Pharmacol.* **158**, 50-60.

Journal of Cell Science